# Mechanism behind the inhibiting effect of $CO_2$ on the oxidation of Al-Mg Alloys

Nicholas Smith[a*], Brian Gleeson[c], Wissam A. Saidi[c], Anne Kvithyld[b], Gabriella Tranell[a]

[a] *Department of Material Science, NTNU, 7034 Trondheim, Norway*
[b] *SINTEF Industry, 7034 Trondheim, Norway*
[c] *Department of Mechanical Engineering and Materials Science, University of Pittsburgh, Pittsburgh, PA 15216, USA*
**Nicholas.Smith@Sintef.no*

**Abstract:** Al-Mg alloys are known to suffer from problematic oxidation during melting, refining and casting. The use of a $CO_2$/air cover gas is known to minimize this oxidation; however, a mechanistic understanding of the beneficial inhibiting effect is lacking. A series of thermogravimetric experiments were conducted under a variety of different $CO_2$-containing atmospheres at 750 °C to elucidate the inhibiting effect. Characterization of the oxide layer was done by surface and cross-sectional analysis in the electron microscope and XPS depth profiling. It was found that additions of as little as 5 % $CO_2$ to air delayed the onset of breakaway oxidation for at least 7 hours and gave a notable reduction in the mass gain compared to exposure to air at 750 °C. The XPS depth profile showed a carbon-containing layer due to adsorbed $CO_2$ at the top surface of the oxide layer. It was inferred that this carbon-containing layer slowed the transport of Mg vapor from the metal through the oxide layer resulting in a reduction in the amount of Mg vapor available for oxidation.

# 1 INTRODUCTION

Al-Mg alloys are known to exhibit excessive oxidation rates, with corresponding melt losses in the casthouses. The addition of Mg to an Al melt has a significant impact on the oxidation rate, as Mg oxidizes preferentially to Al to form a MgO or $MgAl_2O_4$ layer, depending on the Mg content of the alloy[1]. Magnesium is known to segregate to the surface, giving a higher effective Mg content at the metal-oxide interface. Further, it has been shown that the evaporation of Mg from an Al-Mg alloy at elevated temperatures is significant[2], Wightman and Fray[3] deduced that it was Mg transport through the oxide layer that was rate controlling for the oxidation. By contrast, it has also been proposed that the transport of oxygen through the oxide layer is rate controlling[4]. Previous work by the authors on Al-Mg alloys has shown that the diffusion of Mg out is controlling for the oxidation at elevated temperatures. Oxidation of an Al-Mg alloy with 5 % Mg at temperatures above the melting point resulted in an oxide that consisted of two distinct oxide layers, a dense oxide adjacent to the metal that is primarily formed during heating and melting and a granular oxide that forms on top of the dense oxide layer. The granular layer was found to account for the bulk of the oxidation occurring above the melting point[5]. The growth of the granular layer on top of the dense layer was concluded to be due to the oxidation of Mg that had diffused out through the dense oxide layer, due to a significant vapor pressure of Mg at these temperatures.

Al-Mg alloys are known to undergo three distinct stages of oxidation: incubation, breakaway and passivation. The incubation stage is an initial period of low oxidation that is controlled by diffusion through the MgO layer. After a period ranging from a few minutes to hours, depending on alloy composition and oxidation conditions, the MgO layer will rupture, initiating breakaway oxidation, resulting in a dramatic

increase in the oxidation rate and a significant loss of Mg from the alloy due to its vaporization and subsequent oxidation to MgO or $MgAl_2O_4$. The oxidation rate will remain high until most of the Mg in the alloy has been depleted, at which point the rate will decrease to near zero[1]. Gases typically considered to be inert, such as argon or nitrogen, tend to have little effect on the rate of liquid Al-Mg alloy oxidation, as these gases at standard laboratory purity have sufficient amounts of oxygen to allow oxidation to occur[6]. While ppm additions of beryllium to the alloy have been used by the aluminum- producing industry to suppress oxidation, its use presents potential health risks[5]. To that end, reactive cover gases have shown promise as a potential replacement.

$CO_2$ is one such reactive gas that has been shown to reduce the oxidation of Al-Mg alloys[3,4,7,8]. Air-based atmospheres containing as little as 5 % $CO_2$ have been shown to suppress the oxidation of Al-Mg alloys and delay breakaway oxidation. Cochran *et al.*[7] found that the minimum amount of $CO_2$ required to protect an Al-Mg melt from excessive oxidation is proportional to the magnesium content. Haginoya *et al.*[4] carried out a detailed study, to date only published in Japanese, on the effects of $CO_2$ on the oxidation and confirmed that $CO_2$ additions to the atmosphere could slow the oxidation kinetics. Moreover, it was proposed that the inhibiting effect was due to the adsorption of $CO_2$ onto the MgO surface slowing the transport of oxygen to the melt; however, conclusive proof of this was not reported.

The interactions of $CO_2$ with a MgO surface was investigated by Tosoni *et al.*[9] where through density function theory (DFT) simulations it was found that $CO_2$ can adsorb onto the MgO surface and can react to form carbonate and carboxylate species. These results are backed up by the experimental studies of Onishi *et al.*[10] who found that $CO_2$ could adsorb onto the MgO surface and form carbonate species at room temperature. Though these species are not stable at 750 °C it does indicate an interaction between the $CO_2$ molecule and MgO surface. No published work was found on the interaction of $CO_2$ with a bare Al-Mg surface.

**1.1. Thermodynamic considerations.** From a thermodynamic viewpoint, the addition of $CO_2$ to an air atmosphere would not be expected to affect the oxidation of an Al-Mg melt, as both Mg and Al are able to reduce $CO_2$ at the temperature range in question. With the $CO_2$ first being reduced to CO per equations 1 or 3 below, the CO may also be further reduced to C per equation 2 or 4. Mg will oxidize preferentially to Al, however, once all Mg has been oxidized to MgO, the alloy will continue to oxidize to $MgAl_2O_4$[11].

$$\frac{1}{2}Mg + \frac{1}{2}CO_2 = \frac{1}{2}MgO + \frac{1}{2}CO \qquad \Delta G = -296.8 \text{ kJ/mol oxygen at } 750°C \qquad (1)$$

$$Mg + CO = MgO + C \qquad \Delta G = -288.4 \text{ kJ/mol oxygen at } 750°C \qquad (2)$$

$$\frac{1}{3}Al + \frac{1}{2}CO_2 = \frac{1}{6}Al_2O_3 + \frac{1}{2}CO \qquad \Delta G = -257.4 \text{ kJ/mol oxygen at } 750°C \qquad (3)$$

$$\frac{2}{3}Al + CO = \frac{1}{3}Al_2O_3 + C \qquad \Delta G = -249.0 \text{ kJ/mol oxygen at } 750°C \qquad (4)$$

In an atmosphere not containing any free oxygen, the maximum CO partial pressure in the system is controlled by the Boudouard reaction given in equation 5. The equilibrium CO fraction ($CO/CO+CO_2$) is calculated to be 0.78 at 750 °C and will increase as the temperature increases. As CO is only generated from equations 1 and 3, it will take time for the CO partial pressure to reach the level required for it to react in this system either by equation 2, 4 or 5, unless the total amount of gas is limited in relation to the reactant surface area. Under a flowing gas the amount of CO build-up will be limited, which suggests that deposition

of elemental carbon on the surface should not be expected. The addition of oxygen to the system will drive the CO partial pressure down as the CO will be oxidized back to $CO_2$ in accordance with equation 6.

$$CO = \frac{1}{2}C + \frac{1}{2}CO_2 \quad (5)$$

$$\frac{1}{2}CO + \frac{1}{4}O_2 = \frac{1}{2}CO_2 \qquad \Delta G = -193.8 \text{ kJ/mol oxygen at } 750°C \quad (6)$$

In a $CO_2$/air atmosphere, any free oxygen in the system should react with Mg to form MgO per equation 7 or, in the absence of Mg or for very low Mg chemical activity, with Al per equation 8. Based on Graham's law[12] which states that the diffusion rate of a given gas constituent is inversely proportional to the square root of its molecular weight, the flux of $O_2$ from the bulk gas to the oxide layer should occur faster than $CO_2$, for a similar bulk-gas content of these two constituents. Specifically, under a $CO_2$/air atmosphere the sample will have an $N_2$ containing boundary layer which $O_2$ and $CO_2$ must diffuse through before reacting. It is calculated using Graham's law that the $O_2$ flux through this boundary layer will be 1.2 times higher than that of $CO_2$ if the gradients of the two oxidants are the same.

$$Mg + \frac{1}{2}O_2 = MgO \qquad \Delta G = -676.9 \text{ kJ/mol oxygen at } 750°C \quad (7)$$

$$\frac{2}{3}Al + \frac{1}{2}O_2 = \frac{1}{3}Al_2O_3 \qquad \Delta G = -451.3 \text{ kJ/mol oxygen at } 750°C \quad (8)$$

Based on the analysis above it can be surmised that the oxidation inhibiting effect of $CO_2$ is not thermodynamically dictated. Thus, a fundamental understanding of the mechanism and kinetic effects, explaining how $CO_2$ reduces the oxidation is still lacking. The purpose of this work was to elucidate on this mechanism.

# 2 EXPERIMENTAL PROCEDURES

**2.1. Materials.** A model aluminum alloy with a targeted 5 wt. % Mg was prepared by combining appropriate amounts of 99.999 % pure Al and 99.98 % Mg to give a total mass of 147 grams. The mixture was then placed in an alumina crucible and induction melted in an argon atmosphere. The alloy melt was held at 850 °C for 15 minutes to ensure homogenization. The alloy composition was analyzed by ICP-MS and found to contain 4.85 $\pm$ 0.16% Mg. Oxidation samples measuring 10 mm in diameter and 1.5 mm thick were made using a SiC abrasive saw to cut the as-cast alloy to 1.5 mm thick slices, which were then punched to 10 mm discs. Prior to oxidation, samples were polished to a 1 µm finish and stored in ethanol.

**2.2. Oxidation Testing.** A Linseis STA 2400 thermogravimetric analysis (TGA) system with a 10 µg sensitivity was used for the oxidation experiments. For a given test, a sample stored in ethanol was dried, weighed, and placed in the TGA and exposed to a variety of different gas atmospheres. Samples were heated to the oxidation temperature of 750 °C under an argon environment with a heating time of 35 minutes. Once the sample reached 750 °C, the chosen reactant gas was introduced into the chamber and exposure continued for up to 420 minutes. Table 1 outlines the experimental matrix for the main study. Laboratory purity argon (99,999% pure), which contains trace amounts of oxygen, was used for all the experiments. Hence, it must be assumed that the alloy will oxidize to some extent even under such atmosphere.

To better understand the effects of CO on the oxidation, experiments 17-20 were carried out. In these experiments a gas flow of 20%CO/80"Ar was started at the start of heating and stopped once 750 °C was reached. This resulted in a non-flowing atmosphere over the sample. As the gas was not flowing, any formed

CO gas from reaction 1 and 3 remained in the proximity of the sample, allowing the effects of a potentially increasing CO partial pressure to be investigated. A standard total gas flow of 0.2 liters per minute was used for all experiments. Multiple baseline experiments were carried out under different flow conditions to allow mass changes from the apparatus to be differentiated from those due to reactions on the sample. The trace amount of $CO_2$ that are found in air is neglected in this work as the amount is significantly lower that what Cochran *et al.*[8] found to be required to protect an Al-Mg alloy.

**2.3. Sample Analyses.** After oxidation, the percent mass gain vs. time was plotted by dividing the mass change by the initial mass. Mass gain provides clear information about effects of different conditions on the oxidation rate, however, to best understand the mechanism behind the inhibiting effect of $CO_2$, a detailed characterization of the oxide layer morphology was required. This was achieved by analyzing the samples using a FEI Helios NanoLab DualBeam focused ion beam (FIB) miller in which a cross-section was cut through the oxide layer into the base metal such that the morphology and thickness of the oxide layer could be evaluated. To ensure a representative cross-section, the entire surface of the sample was first investigated to find a representative area to make the cross-section, additionally multiple cross-sections from each sample were made. A platinum layer was deposited was deposited on the surface just prior to making a cross-section to protect the oxide layer during sectioning. Selected samples were analyzed in a Joel JEM ARM200F TEM with TEM samples being prepared using the FIB. Finally, to locate any carbon-containing regions on and/or within the oxide layer, a Kratos Axis Ultra DLD X-ray photoelectron spectrometer (XPS) coupled with argon sputtering was used to generate a depth profile through the oxide layer.

### 2.4. Density Functional Theory Calculations

To ensure that no unknown interactions between $CO_2$ and the bare Al-Mg surface were responsible for the inhibiting effect DFT calculations were carried out as described below. DFT simulations were conducted using the Vienna ab-initio simulation package VASP[13,14] employing Perdew-Burke-Ernzerhof (PBE) exchange-correlation functional in all calculations[15]. The electron-nuclear interactions were described using the projector augmented wave (PAW) in which the wave functions are expanded using plane waves with an energy cutoff of 350 eV. The Al(111) surface was modeled using a (3x3) surface supercell based on conventional unit cell (lattice constant 4.04 Å), and eight layers in the non-periodic direction. A vacuum of more than 15 Å was used to mitigate fictitious interactions in the non-periodic direction. A 4x4x1 k-grid was used to sample the Brillouin zone. The energy relaxation was iterated until the forces acting on all of the atoms were less than 1 meV/ Å, with a convergence in the total energy of $10^{-6}$ eV. During optimization of the substrate structures, the four layers from the bottom of the slab were fixed, whereas the other four layers were fully relaxed to their lowest energy configurations with respect to all of the remaining degrees of freedom. The fixed layers were set to their bulk positions using their optimized lattice constants. Validation of the computational framework was done by checking that the energy cutoff, k-grid, energy tolerances were sufficient to converge energy differences to less than 1 meV.

# 3 RESULTS

**3.1. TGA mass gain results.** Results of the experiments are summarized in Table 1. In cases where the atmosphere was changed midway through the oxidation test, the initial gas composition is listed as stage 1 and the new atmosphere is listed as stage 2 as well as the times each atmosphere was present over the sample. Mass gain was calculated by taking the mass difference of the sample between 405 minutes and 5 minutes of oxidation at 750 °C. No traces of deposited Mg vapor were visually observed on the crucible or furnace walls after a given oxidation test. Any mass loss due to Mg evaporation was hence assumed

minimal and could be neglected. Breakaway time was defined by the point where the mass gain departed from a linearity, and was defined equation 9.

$$mass_t - mass_{t-1min} > 0.02 \quad (9)$$

The criterion of 0.02 was decided based on the signal to noise ratio of the TGA used and would vary depending on the apparatus used. The time for breakaway oxidation to begin was generally found to be between 175 and 185 minutes at 750 °C, but varied between 133 and 310 minutes for oxidation in 100 % air.

**Table 1. Results of TGA experiments**

| | Stage 1 | | | Stage 2 | | | Notes | Mass gain (mg) | %Mass gain | Mass gain (mg/cm2) | Breakaway time |
|---|---|---|---|---|---|---|---|---|---|---|---|
| EXP # | Gas 1 | Gas 2 | Time (min) | Gas 3 | Gas 4 | Time (min) | | | | | |
| 1 | 100 Air | | 420 | | | | | 15.03 | 6.23 | 30.69 | 175 |
| 2 | | | | | | | | 2.2 | 0.86 | 4.49 | 310 |
| 3 | 20 CO | 80 Ar | 420 | | | | | 0.31 | 0.13 | 0.63 | >420 min |
| 4 | 5 $CO_2$ | 95 air | 420 | | | | | 0.06 | 0.02 | 0.12 | >420 min |
| 5 | 20 $CO_2$ | 80 air | 420 | | | | | 0.25 | 0.08 | 0.51 | >420 min |
| 6 | | | | | | | | 0.25 | 0.10 | 0.51 | >420 min |
| 7 | 50 $CO_2$ | 50 air | 420 | | | | | 0.32 | 0.12 | 0.65 | >420 min |
| 8 | 20 $CO_2$ | 80 Ar | 420 | | | | | 0.38 | 0.18 | 0.78 | >420 min |
| 9 | 20 $CO_2$ | 80 air | 30 | 100 air | | 390 | | 0.77 | 0.32 | 1.57 | 378 |
| 10 | | | | | | | | 1.35 | 0.58 | 2.76 | 303 |
| 11 | 20 $CO_2$ | 80 air | 60 | 100 air | | 360 | | 0.32 | 0.13 | 0.65 | >420 min |
| 12 | 100 air | | 60 | 20 $CO_2$ | 80 air | 360 | | 0.21 | 0.09 | 0.43 | >420 min |
| 13 | 100 air | | till breakaway | 20 $CO_2$ | 80 air | | | 3.16 | 1.68 | 6.45 | 175 |
| 14 | | | | | | | | 5.63 | 2.91 | 11.50 | 184 |
| 15 | | | | | | | | 2.63 | 1.44 | 5.37 | 133 |
| 16 | 20 $CO_2$ | 80 air | 420 | | | | from start | 0.17 | 0.08 | 0.35 | >420 min |
| 17 | 20 $CO_2$ | 80 air | 420 | | | | Not flowing | 0.46 | 0.22 | 0.94 | >420 min |
| 18 | | | | | | | | 0.28 | 0.14 | 0.57 | >420 min |
| 19 | 20 $CO_2$ | 80 Ar | 420 | | | | Not flowing | 0.89 | 0.33 | 1.82 | >420 min |
| 20 | | | | | | | | 0.5 | 0.27 | 1.02 | >420 min |

For reference experiments 1 and 2 which were carried out in only air, it can be seen that the breakaway time varied significantly. As experiments 13-15 were initially oxidized in air until breakaway occurred the breakaway time for these experiments can be used in addition to experiments 1 and 2 to determine an average breakaway time between 175 and 185 minutes, though it could vary between 133 and 310 minutes. The samples that had a shorter or longer breakaway time are likely attributed to surface defects or inhomogeneity. A mixed $CO_2$/air atmosphere was found to have a strong inhibiting effect on the oxidation of a 5 % Mg-Al alloy compared to an air atmosphere as no sample broke away under a $CO_2$ containing atmosphere. The results from the TGA experiments were found to generally agree with those of Haginoya and Fukusako[4]. Figures 1-5 show the effect of different flow conditions on the percent mass gain. In all the figures the zero point for percent mass gain is set to five minutes after the reactant gas has been switched on, as a significant proportion of the instability in the mass balance, caused by the change in gas flow had stabilized within that time. Figure 1 shows the mass gain of the alloy for increasing amounts of $CO_2$ in air ranging from 5 to 50 % $CO_2$, compared to air (experiments 4-7). It can be seen that while there is a variation in the length of the incubation period for the samples in pure air, the samples oxidized under a $CO_2$-

containing atmosphere remained in the low mass-gain incubation region for all 7 hours. It can also be seen that additions of 5 % $CO_2$ to air protected the alloy equally as well as 50 % $CO_2$ in air, as the variation in the mass gain between the samples is less than one standard deviation. This disagrees with the work by Haginoya *et al.*[4] who found that the amount of $CO_2$ was important. This may be due to the higher Mg content used in that work requiring a higher amount of $CO_2$ to protect the melt.

Figure 2 shows that the mass gain in $CO_2$/Ar (experiment 8) was very similar to $CO_2$/air. This figure also compares the percent mass gain curves for $CO_2$/Ar vs. CO/Ar, where it can be seen that CO provides a similar protective effect when compared to only air.

In experiments 9-11 the samples were initially oxidized in a $CO_2$-containing environment for an initial period after which the $CO_2$ was turned off and oxidation continued in only air. It was found that 30 minutes of $CO_2$ was not sufficient to protect the sample for the entire 7 hours, as those samples exposed initially to $CO_2$ for 30 minutes began to breakaway near the end of the oxidation cycle. However, 60 minutes of initial exposure to $CO_2$ was sufficient to protect the sample for 7 hours, as shown in Figure 3.

Figure 4 shows the results of samples that were initially oxidized in only air for a short period followed by oxidation in $CO_2$/air (experiments 12-15). Addition of $CO_2$ to the atmosphere shortly after the onset of breakaway oxidation (experiments 13-15) was found to provide a protective effect and resulted in the suppression of breakaway oxidation. The ability to suppress breakaway oxidation is time dependent, in that if $CO_2$ is not introduced in the early stage of breakaway oxidation it appears to have a limited effect on the oxidation (experiment 14), as can be seen in Figure 4. Oxidation in pure air for 60 minutes followed by 20$CO_2$/80air (experiment 12) showed similar mass gain to samples oxidized for the entire holding period in a $CO_2$ atmosphere.

Experiments 1-16 were done under an atmosphere that was flowing, and therefore had a constant $CO_2$ and CO partial pressures over the sample surface. In experiments 17-20, the furnace was filled with 20$CO_2$/80air and sealed for the duration of the experiment, thus allowing the $CO_2$ and CO partial pressures to vary with time. The results from these experiments are shown in Figure 5, where it can be seen that the mass gain was slightly higher in the experiments where the gas was not flowing. Further, the 20$CO_2$/80Ar samples had an average mass gain of 1.42mg/cm$^2$ versus 0.76 mg/cm$^2$ for 20$CO_2$/80Air.

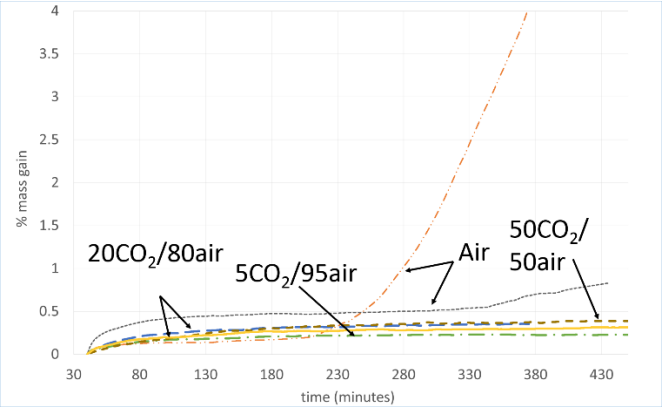

**Figure 1.** Effects of varying amount of $CO_2$ in air compared to oxidation in pure air (experiment numbers 1-2, 4-7).

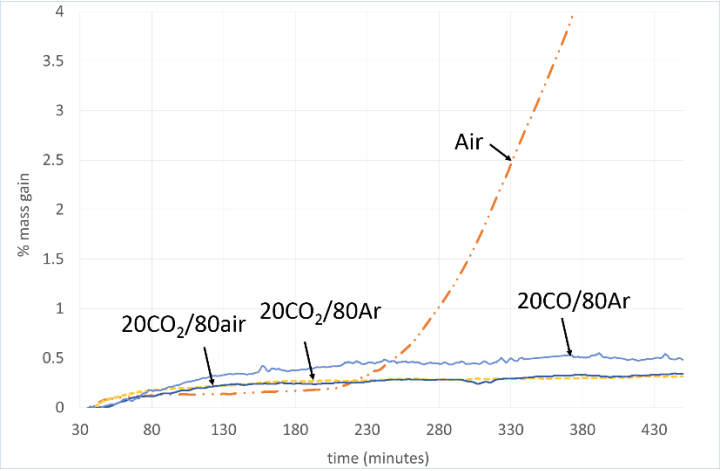


**Figure 2.** Similarities between $20CO_2/80air$, $20CO_2/80Ar$ and $20CO/80Ar$ (experiment numbers 1, 3, 5, 8).

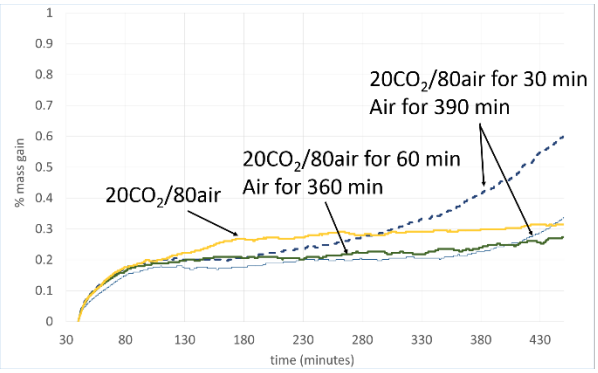


**Figure 3.** Effects of $CO_2$ for a short period at start of the oxidation cycle followed by air only (experiment numbers 5, 9-11).

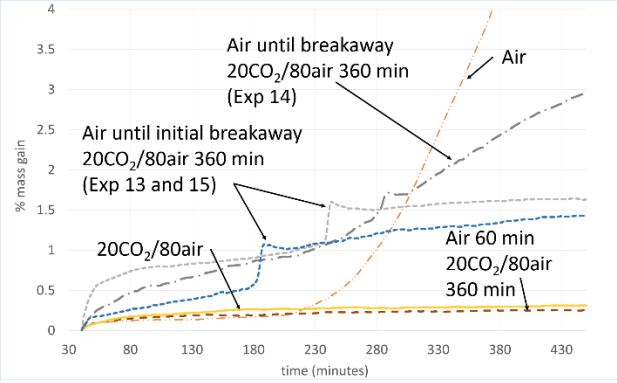

**Figure 4.** Effects of $CO_2$ additions after a period of oxidation in only air (experiment numbers 1, 5, 12-15).

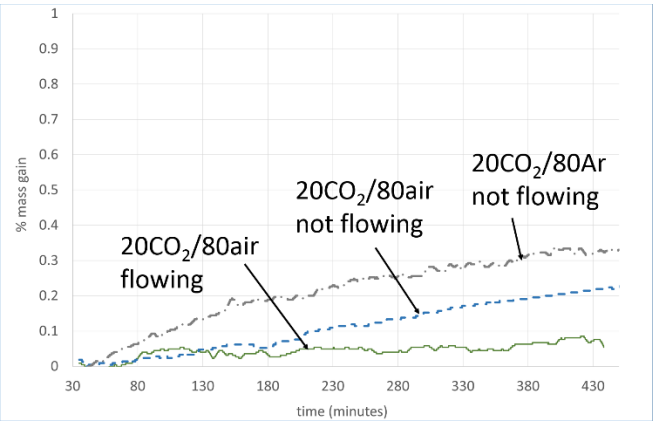


**Figure 5.** Effects of a non-flowing atmosphere on the mass gain (experiment numbers 16-20).

**3.2. Oxide Layer Morphology.** From a comparison between the oxide layers on the samples oxidized in a $CO_2$-containing atmosphere and those in pure air, it has been observed that the addition of $CO_2$ limits the formation of a granular layer at the surface of the oxide layer. This granular layer has previously been seen to form as a result of the oxidation of Mg vapor that had diffused through the oxide layer of an Al-Mg alloys at elevated temperatures. The absence of the granular layer indicates that the diffusion of Mg through the oxide layer has been significantly reduced[5].

As a reference, a sample heated in argon and held at 750 °C for 1 minute was found to have a 60 nm thick oxide layer, indicating that an appreciable amount of oxidation occurred during the 35 minutes required to heat and melt the samples, this should be considered as the initial oxide layer thickness for the discussion below. Examination in the FIB showed that cracks in the oxide layer were present for all the samples after oxidation. In general, the cracks appeared to be covered by an oxide layer under 10 nm thick, as indicated in Figure 6 showing a both the surface and cross-section of a crack after oxidation in $20CO_2$/80Air at 750 °C for 60 minutes. For samples that were oxidized in $CO_2$ for a short period followed by oxidation in pure air (experiments 9-11), many of the oxide cracks were filled completely with oxide, as shown in Figure 7. It is inferred that these cracks formed when the alloy melted and that subsequent oxidation in the cracks was limited by the presence of $CO_2$, resulting in an oxide layer of approximately 10 nm thick.

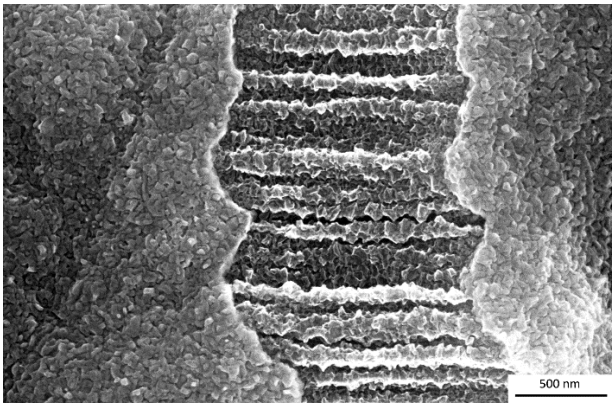

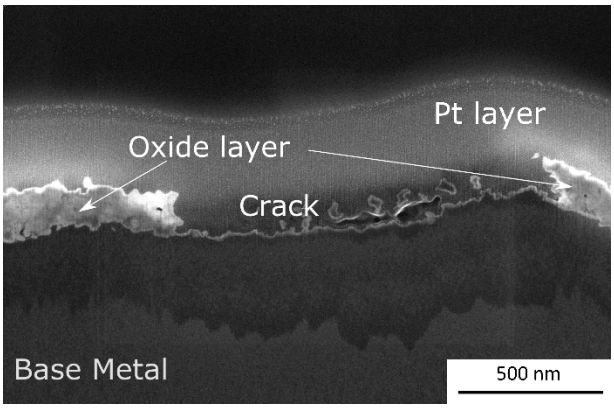


**Figure 6.** Top surface and cross-section of crack on sample oxidized for 60 min in 20$CO_2$/80Air at 750 °C.

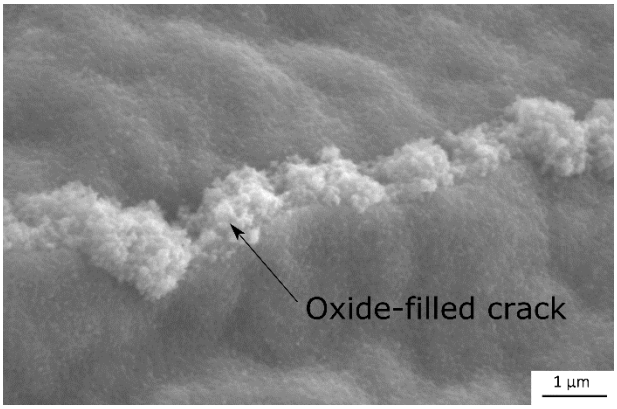


**Figure 7.** Crack filled with oxide after 30 min in 20$CO_2$/80air followed by 390 min in pure air at 750°C.

Cross-sectional TEM examination of samples oxidized under a $CO_2$ containing atmosphere showed that the oxide layer is comprised of small grains measuring 35 nm ±20 nm in size. Electron energy loss spectroscopy (EELS) revealed that the oxide layer consisted of MgO with no indication of aluminum oxide, spinel or carbon present.

While the mass-change results showed little difference between samples oxidized in 20$CO_2$/80air and 20$CO_2$/80Ar, a minor difference in the morphology of the layers was found. The layer on the sample oxidized in $CO_2$/Ar had a regions that were covered in a granular layer at the gas-oxide interface, as seen in Figure 8. The majority of the sample did not appear to form this granular layer, as seen in Figure 9, but instead formed a similar-structured oxide layer as found on samples oxidized in $CO_2$/Air as seen in Figure 6.

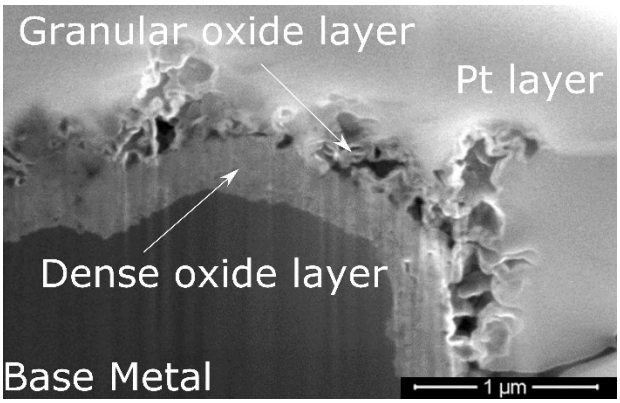


**Figure 8.** Cross-section of sample with a dense layer covered by a granular layer after oxidization in $20CO_2/80Ar$ for 420 min at 750 °C.

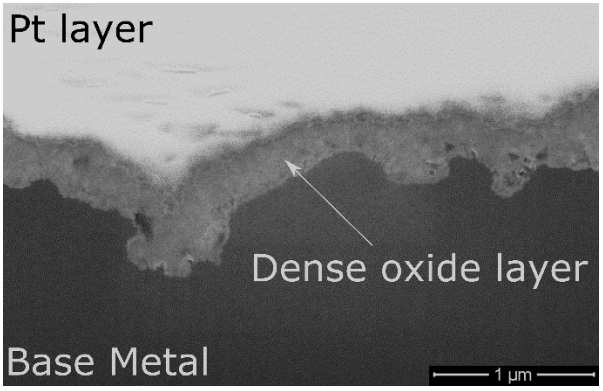


**Figure 9.** Sample oxidized in $20CO_2/80Ar$ for 420 min at 750°C with no granular layer preset (same sample as Figure 8).

**3.3. XPS depth profile.** The high amount of topography of the samples oxidized at 750 °C resulted in less than ideal conditions for an XPS depth profile. To overcome this, a sample was oxidized at 550°C for 420 minutes in $20CO_2/80Ar$ with the aim of creating a smooth surface for XPS. However, an Mg-rich phase existed in the sample and at 550 °C this phase exhibited extensive oxidation, resulting in a granular oxide layer that was 3 µm thick on average as shown in Figure 10, but was up to 10 µm thick in selected locations. It is deduced that at 550°C the oxygen partial pressure in the Ar was not sufficient to form a dense oxide layer like that seen on samples exposed at 750 °C. Due to the thickness of the oxide layer formed at 550 °C, it was not possible to sputter through the entire oxide layer into the base metal. As a result only the top 2 µm of the oxide layer were examined.

The overall depth profile is shown in Figure 11. Here it can be seen that the oxide layer is primarily MgO, however, increasing amounts of Al and $MgAl_2O_4$ can be found with increasing depths. The minor oscillations in the curve are attributed to minor variations in the structure of the granular oxide.

The oxygen signal was interpreted to be comprised of three peaks: oxygen associated with MgO; oxygen associated with $MgAl_2O_4$; and oxygen associated with carbon. The ionic Mg and Al peaks stemming from the oxides were clear and well defined, allowing the amount of oxygen associated with those oxides to be subtracted, leaving a clear peak showing the oxygen that must be associated with the carbon.

Analysis of the carbon peak showed that the carbon signal was comprised of four peaks, as shown in Figure 12. Figure 13 shows the depth profile from the carbon signal and the associated oxygen signal. The oxygen signal is believed to be primarily associated with the peak at 286.4 eV. Initially a 2:1 ratio is seen between the oxygen and C 286.14 eV signal, which would strongly indicate the presence of adsorbed $CO_2$. The oxygen signal decreases as the depth into the oxide layer increases, and the O:C ratio at the end of the profile becomes 1:1. This decrease in oxygen is likely due to the adsorbed $CO_2$ being reduced to CO by Mg inside the oxide layer.

The peak at 291.5 eV is at a similar position to the one reported by Onishi *et al.*[12] after exposure of MgO to $CO_2$ at room temperature. It was suggested by these authors that this is the magnesium carbonate peak; however, thermodynamic calculations show that magnesium carbonate should not form on samples at the temperatures used in this work. It is speculated that this carbonate formed when the sample cooled after the isothermal exposure. The two unknown carbon peaks are at too high of binding energies to be elemental carbon or a carbide phase[16] and their source is currently unknown.

An XPS profile from a sample oxidized at 750 °C was generated, but as explained above, the topography made it difficult to obtain an accurate depth profile. The carbon signal from the 750 °C sample is shown in Figure 14. This signal is from after the top nanometers have been sputtered away to remove any surface contamination. It can be seen that the general shape of the curve is the same as that of the 550 °C sample. Therefore, it can be assumed that similar carbon species will exist on a sample from 750 °C as was found at 550 °C.

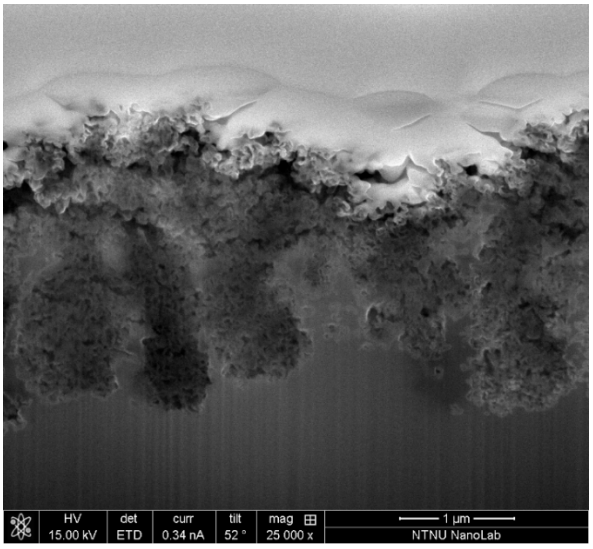


**Figure 10.** Oxide layer on sample oxidized at 550°C in $20CO_2/80Ar$ for 420 minutes and analyzed by XPS.

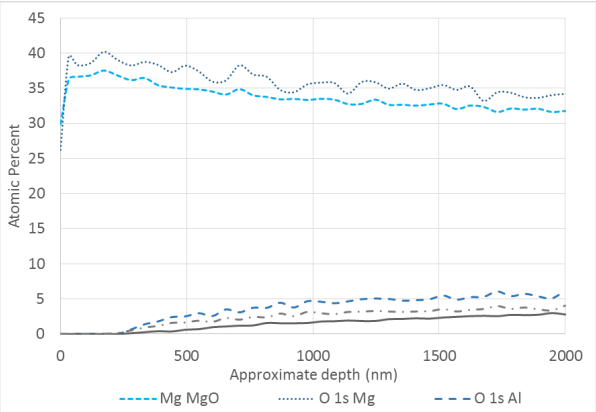


**Figure 11.** XPS depth profile of Mg and Al for sample oxidized at 550°C.

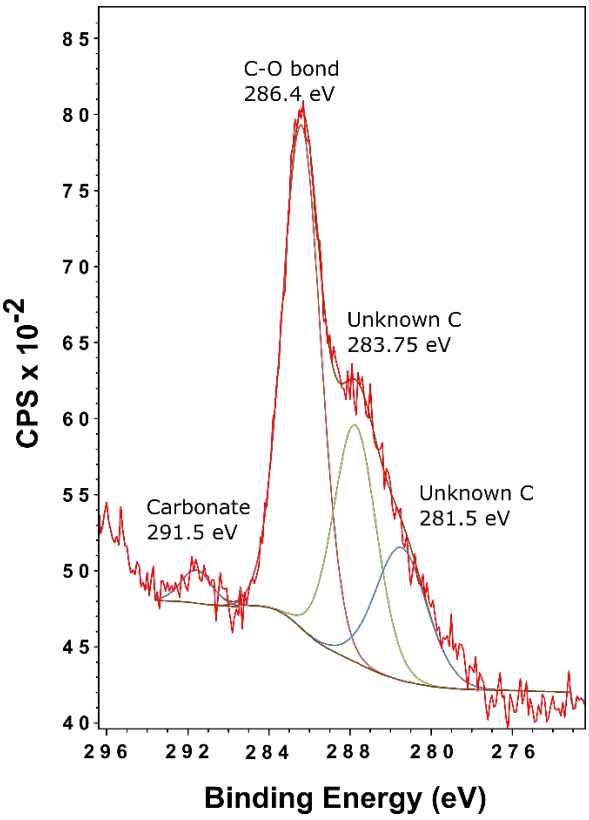


**Figure 12.** Carbon peak from 172 nm depth of the 550 °C sample.

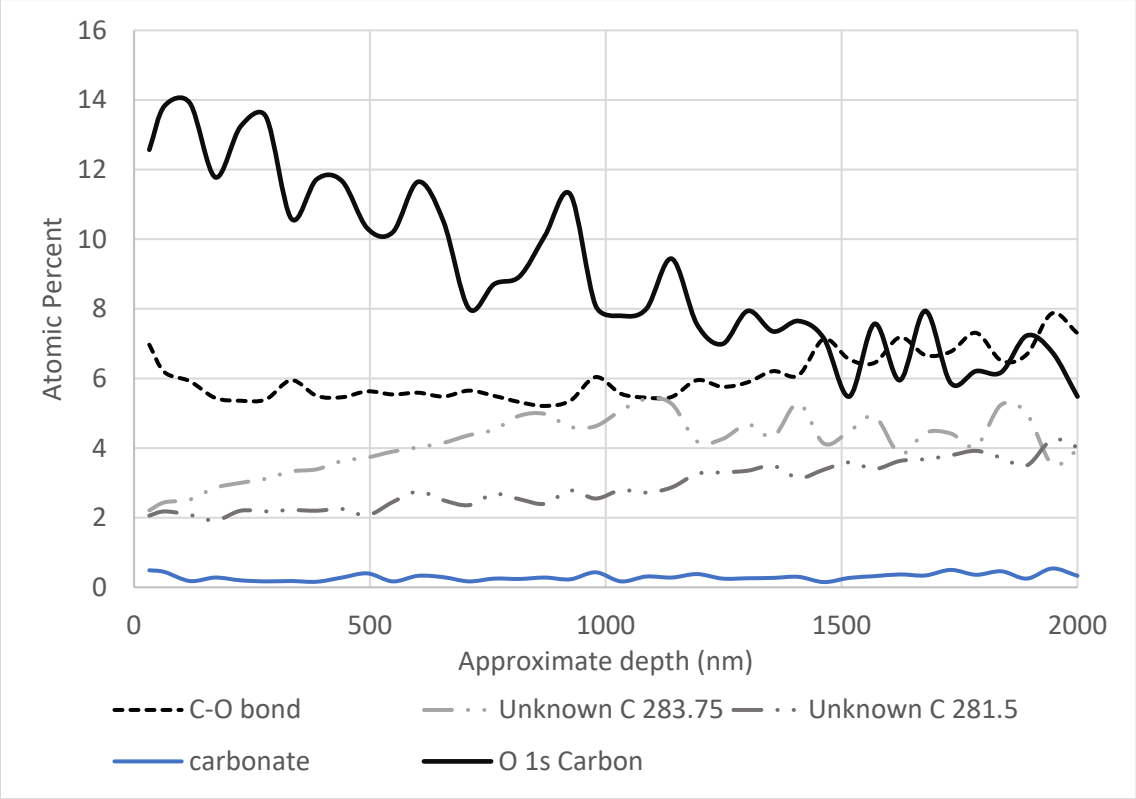


**Figure 13.** Depth profile of carbon and the associated oxygen signal from sample oxidized at 550°C in air.

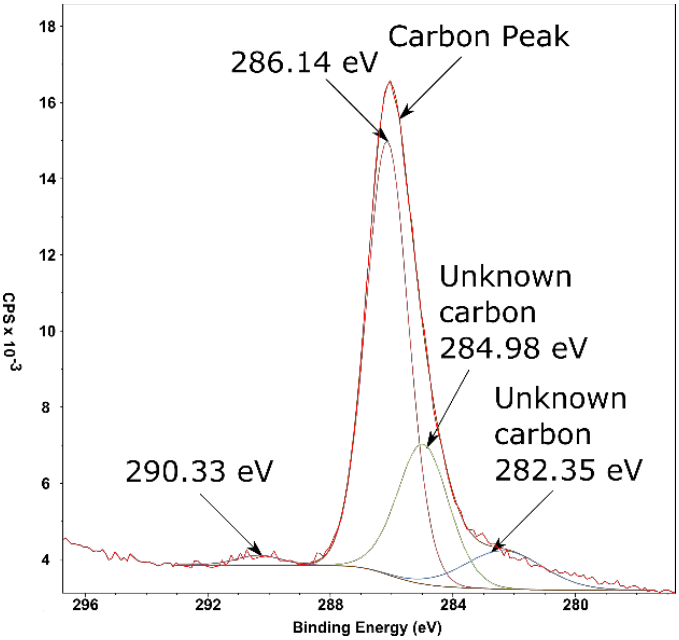


**Figure 14.** XPS carbon peak from oxidation at 750 °C after initial surface has been sputtered away.

The DFT calculations, in agreement with thermodynamic predictions, show that the interactions of oxygen with either pristine or Mg-doped Al(111) surface is a significantly more favorable with $O_2$ than with $CO_2$. This indicates that directly preferential reaction/adsorption of $CO_2$ on the metal surface is not likely unless the $CO_2$ sticking probability is greater than that of oxygen. Previous studies have showed that the oxygen sticking probability on Al(111) is very low despite strong adsorption energies. This is due to spin selection rules associated with the triplet spin state of $O_2$ (g), which results in a highly nonadiabatic behavior in the oxygen/Al(111) interactions[17]. On the other hand, $CO_2$ is in a singlet spin arrangement in its ground state and hence is not affected by the spin selection rules as it dissociates on the Mg-doped Al(111) surface. This shows that $CO_2$ may adsorb onto the alloy surface preferentially to oxygen.

# 4 DISCUSSION

**4.1. Effects of CO presence.** In experiments 17-20 where the gas was held static over the sample, a slightly higher mass gain was recorded in $CO_2$/Ar than in $CO_2$/Air. While the average difference is small it does indicate that the oxidation is dependent on the CO partial pressure. When the oxidation occurs in a $CO_2$/air environment, any formed CO will be oxidized back to $CO_2$ in the gas phase per equation 6, thus maintaining a low CO partial pressure; however, for oxidation in a $CO_2$/Ar atmosphere the CO partial pressure will increase with increased time, resulting in an increase in oxidation.

This is likely due to differences in how CO interacts with the oxide surface. However, CO must interact with the surface in a way that will inhibit the oxidation, as the overall mass gain in CO/Air was still lower than when the oxidation took place in only air. The work by Wightman *et al.*[3] showed that oxidation in $CO_2$ is independent of $CO_2$ concentration, but the reaction of CO with Mg (equation 2) is dependent on the CO concentration. This would support the conclusion from this work that the CO partial pressure is important to the oxidation rate.

**4.2. Proposed mechanism.** In order to understand the mechanism by which $CO_2$ reduces the oxidation rate, we summarize and consider the physical evidence gathered in this work:

- The granular layer on the surface of the dense MgO layer is not found with the addition of $CO_2$ to an air atmosphere.
- $CO_2$ quickly slows down oxidation when added to the atmosphere prior to the onset of breakaway.
- The effect of $CO_2$ in the atmosphere "lingers" when removed.
- The O:C ratio at the top MgO surface corresponds to that of $CO_2$.
- The O:C ratio decreases throughout the MgO oxide layer towards the oxide/metal interface.

Base on the evidence stated above, it is proposed that when a $CO_2$ molecule interacts with the MgO layer it will adsorb onto the surface. The oxide layer will continue to grow around this adsorbed $CO_2$ and eventually result in a decreased oxygen partial pressure below the oxide surface. The adsorbed $CO_2$ will then react with the Mg to form an Mg-O-C phase that has a different structure to the MgO formed in the absence of $CO_2$. This MgO layer that contains adsorbed $CO_2$ and other C-O bonds must modify the physical structure of the layer to form a "cap" at the surface of the oxide layer that reduces the rate of Mg diffusion out.

The immediate observed effect of adding $CO_2$ means that the adsorption is fast. Further evidence of the rapid adsorption can be taken from Figure 6, where the oxide thickness in the cracks was significantly reduced compared to un-cracked oxide, showing that any fresh metal that is exposed will be quickly passivated by the $CO_2$ before significant oxide growth can occur. The lingering effect is likely due to the slow oxidation of the carbon atoms in the structure as oxygen is allowed to diffuse into the structure, gradually opening pores in the oxide layer again and forming a layer that is more open to diffusion, allowing Mg vapor to escape.

**4.3. $CO_2$'s effect on breakaway oxidation.** The ability of $CO_2$ to stop the initial stages of breakaway oxidation can be explained by a lack of available oxygen for the spinel formation. It can be assumed that the diffusion of oxygen from the gas phase into and through the oxide layer must be slowed to a similar extent as the Mg vapor diffusion out was slowed. If the diffusion of oxygen inward is restricted, the only other source of oxygen for the spinel phase formation is via equation 10 below, with the existing MgO layer. However, the Gibbs energy for this reaction is positive at 750 °C as Al cannot reduce MgO at 750 °C, and therefore the spinel phase cannot form via the reaction between Al metal and MgO. Further, as the Mg metal will be trapped in the oxide layer by the carbon containing oxide layer, the Mg activity in the oxide layer increase. As the activity of Mg must be below 0.023 for the spinel phase to form[9], any increase in the activity will inhibit the spinel formation. If the $CO_2$ is added too late in the breakaway period the spinel phase will have already resulted in damage to the oxide layer allowing the direct flux of oxygen into the melt, which will cause the spinel phase to form via equation 11.

$$MgO + \frac{1}{2}Al = \frac{1}{4}MgAl_2O_4 + \frac{3}{4}Mg \qquad \Delta G = 22.1 \text{ kJ/mol oxygen at } 750°C \qquad (10)$$

$$\frac{1}{4}MgO + \frac{1}{2}Al + \frac{3}{8}O_2 = \frac{1}{4}MgAl_2O_4 \qquad \Delta G = -485.6 \text{ kJ/mol oxygen at } 750°C \qquad (11)$$

# 5 CONCLUSION

The effects of an atmosphere containing $CO_2$ on the oxidation of an Al-Mg alloy was investigated experimentally and supplemented with DFT calculations to better understand the mechanism behind the previously-observed inhibiting effect. It was confirmed that addition of as little as 5 % $CO_2$ to air provides a significant inhibiting effect on the oxidation of Al-Mg alloys with the addition of $CO_2$ to air delaying the onset of breakaway oxidation and reducing the overall mass loss due to oxidation. Further, it was shown through DFT calculations that the interaction between the bare Al-Mg surface and $CO_2$ is not responsible for the inhibiting effect.

This inhibiting effect is attributed to the presence of an adsorbed $CO_2$ layer on the thermally grown MgO layer; this adsorbed $CO_2$ reacts with the Mg vapor diffusing out through the oxide layer. The structure of the resulting oxide layer is such that it acts as a physical barrier to further diffusion of Mg vapor out. Further, it was found that:

- Varying the $CO_2$ partial pressures between 5 and 50 % did not influence the inhibiting effect for the same Mg content.
- Under a non-flowing atmosphere $CO_2$/Ar resulted in a higher mass gain than $CO_2$/air, indicating that a low CO partial pressure aids in inhibiting the oxidation.

- Further breakaway oxidation could be suppressed if $CO_2$ is added to the atmosphere during the initial stage of breakaway.
- The inhibiting effects of $CO_2$ will remain for a period of time after the $CO_2$ has been removed from the atmosphere.

# ACKNOWLEDGEMENTS

This paper has been funded by the SFI Metal Production, (Centre for Research-based Innovation, 237738). The authors gratefully acknowledge the financial support from the Research Council of Norway and the partners of the SFI Metal Production. The computational work is supported by the University of Pittsburgh Center for Research Computing through the resources provided.

# REFERENCES

(1) Haginoya, I.; Fukusako, T. Oxidation of Molten Al-Mg Alloys. *Transactions of the Japan Institute of Metals*. **1983**, 24, 613.

(2) Lea, C.; Molinari, C. Magnesium Diffusion, Surface Segregation and Oxidation in Al-Mg alloys. *J. Mater. Sci*. **1984**, 19, 2336.

(3) Wightman, G.; Fray, D.J. The Dynamic Oxidation of Aluminum. *Metall. Mater. Trans. B*. **1983**, 14, 625.

(4) Haginoya, I.; Fukusako, T. Function of $CO_2$ Gas on the Suppression of Oxidation of Molten Al-Mg Alloy. *Journal of Japan Insitute of Light Metals*. **1981**, 31, 733.

(5) Smith, N.; Kvithyld, A.; Tranell, G. The Mechanisim Behind the Oxidation Protection of High Mg Al Alloys with Beryllium. *Metall. Mater. Trans. B.* **2018**, 49, 2846.

(6) Bao S. Filtration of Aluminum-Experiments, Wetting and Modelling. Ph.D. Dissertation, Norwegian University of Science and Technology. Trondhiem, Norway, 2011.

(7) Cochran, C.N.; Belitskus, D.L.; Kinosz, D.L. Oxidation of Aluminum-Magnesium Melts in Air, Oxygen, Flue Gas and Carbon Dioxide. *Metall. Mater. Trans. B*. **1977**, 8, 323.

(8) Tenório, J.A.; Espinosa, D.C. High-Temperature Oxidation of Al-Mg Alloys. *Oxid. Met.* **2000**, 3, 361.

(9) Tosoni, S.; Spinnato, D.; Pacchioni, G. DFT Study of $CO_2$ Activation on Doped and Ultrathin MgO Films. *J.Phys. Chem.* **2015**, 119, 27594.

(10) Onishi, H.; Egawa, C.; Aruga, T.; Iwasawa, Y. Adsorption of Na Atoms and Oxygen-Containing Molecules on MgO(100) and (111) Surfaces. *Surf. Sci.* **1987**, 191, 497.

(11) Surla, K.; Valdiveso, F.; Pijolat, M.; Soustelle, M.; Prin, M. Kinetic Study of the Oxidation by Oxygen of Liquid Al-Mg 5% Alloys. *Solid State Ionics*. **2001**, 143, 355.

(12) Mason, E.A.; Kronstadt, B. Graham's Laws of Diffusion and Effusion. *J. Chem. Educ*. **1967**, 44, 740.

(13) Blochl, P.E. Projector Augmented-Wave Method. *Phys. Rev. B: Condens. Matter Mater. Phys*. **1994**, 50, 17953.

(14) Perdew, J.P.; Burke, K.; Ernzerhof, M. Generalized Gradiant Approximation Made Simple. *Phys. Rev. Lett.* **1996**, 77, 3865.

(15) Kresse, G.; Joubert, D. From Ultrasoft Pseudopotentials to the Projector Augmented-Wave Method. *Phys. Rev. B: Condens. Matter Mater. Phys.* **1999**, 59, 1758.

(16) Barr, T.L.; Seal, S. Nature of the use of Adventitious Carbon as a Binding Energy Standard. *J. Vac. Sci. Technol. A.* **1995**, 13, 1239.

(17) Behler, J.; Delley, B.; Lorenz, S.; Reuter, K.; Scheffler, M. Dissociation of $O_2$ at Al(111): The Role of Spin Selection Rules. *Phys. Rev.Lett*. **2005**, 94, 036104.

For Table of Contents Only